ARTICLES
DOI: 10.1038/s41566-017-0008-0
nature photonics

Control of light by curved space in nanophotonic structures

Rivka Bekenstein[1,2,3]*, Yossef Kabessa[4]*, Yonatan Sharabi[1], Or Tal[1], Nader Engheta[5], Gadi Eisenstein[6], Aharon J. Agranat[4] and Mordechai Segev[1]

Nanophotonics is based on the ability to construct structures with specific spatial distributions of the refractive index. Conventional nanophotonic structures are fabricated in planar settings, similar to electronic integrated circuits. We present a new class of nanophotonic structures with intricate design in three dimensions inspired by general relativity concepts, where the evolution of light is controlled through the space curvature of the medium. We demonstrate this concept by studying the evolution of light in a paraboloid structure inspired by the Schwarzschild metric describing the space surrounding a massive black hole. Our construction allows control over the trajectories, the diffraction properties and the phase and group velocities of wavepackets propagating within the curved-space structure. Finally, our structure exhibits tunnelling through an electromagnetic bottleneck by transforming guided modes into radiation modes and back. This generic concept can serve as the basis for curved nanophotonics and can be employed in integrated photonic circuits.

For decades, general relativity (GR) phenomena have provided exciting inspiration in the field of electromagnetism, as reflected in the famous statement by Landau and Lifshitz: 'We may say that, with respect to its effect on the electromagnetic field, a static gravitational field plays the role of a medium with electric and magnetic permeabilities ε, μ'[1]. However, for a long time no technology could implement GR concepts in optics. Starting in 2000, the rapid development of the field of metamaterials suggested emulation of GR phenomena for optical applications as one of its main routes[2,3]. These applications include, in particular, superlenses[4] and cloaking schemes[5–8], the realization of which often requires negative-refractive-index metamaterials[9] and epsilon near-zero media[10–12]. However, the fabrication of materials with specific inhomogeneous optical properties is still a major challenge, especially for operation in the visible-light regime. This challenge has been addressed by using various methods ranging from tailoring combinations of different materials at nanoscale resolution[7] to the development of alternative plasmonic materials[13]. Because these settings use traditional 2D fabrication techniques, they generally do not exploit the ability to create true curved space in 3D systems[14]. In the past few years, curved-space photonic settings have been studied in experiments with curved surface waveguides coating 3D bodies[15–17]. However, these pioneering experiments were only carried out in macroscopic systems, always in the paraxial regime, and for 3D bodies whose curvature varies slowly with respect to the wavelength. Now, with new abilities to construct 3D curved structures with nanometric resolution, it is intriguing to study what happens when the 3D photonic structures have features comparable to the wavelength of the light propagating within them.

We demonstrate our methodology by designing a hollow paraboloid structure inspired by the most famous solution of Einstein's equations of GR—the Schwarzschild metric—which describes the space surrounding a massive black hole. Several theoretical studies have explored the evolution of light near emulated black holes using transformation optics[18–21], and several optical systems have succeeded in emulating other GR phenomena[22–29]. However, implementing these ideas typically requires complicated fabrication of subwavelength-structured inhomogeneous materials[18–21,26], which heavily relies on 2D fabrication techniques imported from microelectronics. Here, we use a new fabrication technique—relying on multiphoton polymerization—that enables the construction of arbitrary 3D structures with subwavelength features[30]. With this technique we fabricated a 3D waveguide inspired by the static Schwarzschild metric. The ability to explore the propagation of waves in this 3D structure in experiments raises extremely intriguing questions, such as what would happen when the typical size of a curved waveguide (or the emulated Schwarzschild radius) is comparable to the wavelength scale and how would the phase and group velocities of the light be affected by the curvature of space?

To address such questions, and to actually exploit the unique features of light propagating in 3D curved space, we demonstrate a new platform for nano-optics in curved space. We control the curvature and the geometry of a curved waveguide within which light is confined, rather than controlling the optical properties of the medium, as is commonly done for metamaterials. In our setting, the light is restricted to propagating in a predesigned thin manifold embedded in a 3D volume. We study the evolution of light in curved planar waveguides that can be mapped to specific curved space metrics. We explore the properties of light propagating in our curved-space nanophotonic structure, specifically the diffraction and trajectories of optical wavepackets. We find that our system facilitates control over the phase and group velocities of the electromagnetic (EM) waves, exclusively by designing the curvature of space. Finally, we show that our structure

[1]Physics Department and Solid State Institute, Technion, 32000 Haifa, Israel. [2]Physics Department, Harvard University, Cambridge, MA 02138, USA. [3]ITAMP, Harvard-Smithsonian Center for Astrophysics, Cambridge, MA 02138, USA. [4]Department of Applied Physics and the Brojde Center for Innovative Engineering and Computer Science, The Hebrew University of Jerusalem, 91904 Jerusalem, Israel. [5]Department of Electrical and Systems Engineering, University of Pennsylvania, Philadelphia, PA 19104, USA. [6]Electrical Engineering Department, Technion, 32000 Haifa, Israel. Rivka Bekenstein and Yossef Kabessa contributed equally to this work. *e-mail: rivka.bekenstein@cfa.harvard.edu; yossi.kabessa@mail.huji.ac.il

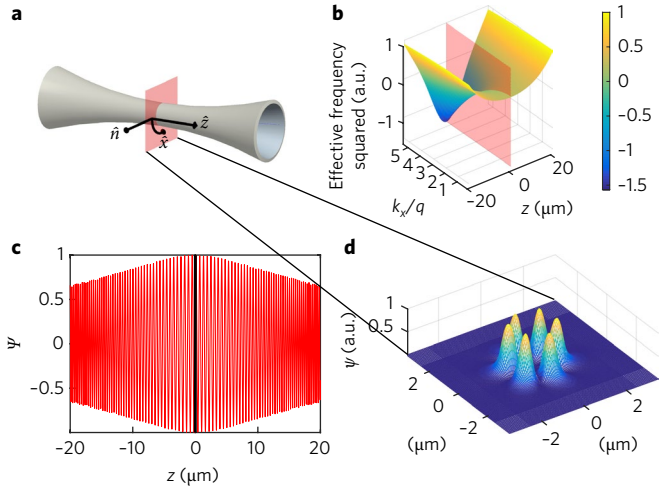

Fig. 1 | Evolution of the modes in the Flamm paraboloid. a, Schematic of the paraboloid waveguide mapped to the Schwarzschild metric. The plane of the emulated Schwarzschild radius ($z=0$) is marked in red. **b**, Normalized effective frequency squared as a function of the spatial frequency and z. When light is launched into this structure from the left, after some propagation distance some modes become unbound as their frequency becomes imaginary. These modes are transformed into radiative modes (Fig. 4). **c**, The electric field envelope $\psi(z)$ of the mode with $k_x=0.9q$. This mode accumulates phase increasingly more slowly as it propagates (in z) toward the emulated Schwarzschild radius (black line), while its spatial frequency in the transverse direction x is growing. **d**, Cross-section of the electric field distribution for a specific z (extracted from FDTD simulations) of a particular mode propagating inside the paraboloid waveguide.

exhibits tunnelling through an EM bottleneck by transforming guided modes into radiation modes and back. The general method of controlling the features of EM waves through a fabricated nanophotonic curved space structure, as demonstrated here, can be the basis for a new type of nanophotonic device. Specifically, the fabrication technique presented here, which relies on Nanoscribe technology[30], allows the construction of any arbitrarily designed curvature and geometry. Thus, we envision that the concepts outlined here can be used in the arena of integrated photonic circuits, as the vehicle for delivering and extracting light to and from very small spaces and as a general technique for creating intricate 3D nanophotonic circuitry.

Interestingly, the spatial Schwarzschild metric can be mapped onto a surface of revolution—Flamm's paraboloid. This is done by considering the known Schwarzschild metric in static time and limiting the space to two dimensions. Specifically, only the space outside the Schwarzschild radius is mapped to the surface of a paraboloid defined by a specific metric (for details see Supplementary Section 1). Consider a thin surface waveguide, in the shape of Flamm's paraboloid, by confining the light to propagate only inside the waveguide we restrict the light to the curved-space background (Fig. 1a). As explained below, we fabricate this waveguide while leaving its interior hollow. As sketched in Fig. 1a, the waveguide looks like two opposing funnels connected at their narrowest point, realizing the geometry of two opposing Flamm paraboloids. The narrowest point—the bottleneck—is mapped to the Schwarzschild radius ($r=r_S$ in Schwarzschild space is mapped to $z=0$ in the paraboloid).

Nonparaxial evolution of EM waves in Flamm's paraboloid

First, we study theoretically the propagation of light in this curved space setting. The dynamics of EM waves in static curved space is described exactly by the Maxwell equations in general coordinates (3D + 1)[1]:

$$\frac{1}{2\sqrt{g}}\varepsilon^{\alpha\beta\gamma}\left(\frac{\partial E_\gamma}{\partial x^\beta}-\frac{\partial E_\beta}{\partial x^\gamma}\right)+\frac{1}{c}\frac{\partial B^\alpha}{\partial t}=0 \qquad \frac{1}{\sqrt{g}}\frac{\partial}{\partial x^\alpha}(\sqrt{g}B^\alpha)=0$$
$$\frac{1}{2\sqrt{g}}\varepsilon^{\alpha\beta\gamma}\left(\frac{\partial H_\gamma}{\partial x^\beta}-\frac{\partial H_\beta}{\partial x^\gamma}\right)-\frac{1}{c}\frac{\partial D^\alpha}{\partial t}=0 \qquad \frac{1}{\sqrt{g}}\frac{\partial}{\partial x^\alpha}(\sqrt{g}D^\alpha)=0 \tag{1}$$

Here, g is the time-independent spatial metric determinant, where $ds^2=g_{\alpha\beta}dx^\alpha dx^\beta$ (α, β and γ are spatial indices, from 1 to 3), $\varepsilon^{\alpha\beta\gamma}$ is the antisymmetric Levi–Civita tensor, and E^α, H^α, D^α and B^α are three vectors representing the electric and magnetic fields and their displacements, respectively, as appears in Maxwell's equations.

First, we introduce the metric of surfaces of revolution (surfaces with axial symmetry). Surfaces of revolution can be parameterized by $\mathbf{s}(u,v)=(\alpha(u)\cos(v),\alpha(u)\sin(v),\beta(u))$, where $v=[-\pi,\pi]$ is the azimuthal angle and $-\infty<u<\infty$ is a general parameterization of the surface along its axis of revolution. Every point in 3D space ($\mathbf{r}$) can be described by the two coordinates on the curved surface (u, v) and a third coordinate (h) normal to the surface at every point: $\mathbf{r}(u,v,h)=\mathbf{s}(u,v)+h\hat{n}(u,v)$, where $\hat{n}(u,v)$ is the unit vector normal to the surface. To simplify the metric terms, we transform to a new set of coordinates: $z=\int_0^z\sqrt{\alpha'^2(u)+\beta'^2(u)}\,du$ and $x=R_0v$, where R_0 is defined by the radius of the surface at $z=0$, namely, x is proportional to the azimuthal coordinate having length units at $z=0$. In this coordinate system, z is the propagation direction, which is also the axis that defines the axial symmetry, and x is the transverse coordinate (see schematic in Fig. 1a).

The line element takes the form

$$dl^2=dz^2+[\alpha^2(u(z))/R_0{}^2]dx^2=dz^2+\gamma(z)dx^2$$

Specifically for the Flamm paraboloid we find

$$dl^2=dz^2+\left(\frac{z^2}{4r_S{}^2}+1\right)^2dx^2 \tag{2}$$

where $\gamma(z)=\left(\frac{z^2}{4r_S{}^2}+1\right)^2$ is the dimensionless 2D determinant and r_S is the Schwarzschild radius of the black hole (see Supplementary Section 1), which relates to the mass of the black hole and is the only parameter distinguishing between different black holes. In our spatial system, r_S relates to the geometrical parameters of the paraboloid. In the analytical approach, we assume[26] that the curvature of space varies slowly with respect to the wavelength and derive a nonparaxial wave equation for continuous waves propagating in the surface. For the transverse electric (TE)-polarized modes, the electric field has no z component, so they are strictly x-polarized, in the form $\mathbf{E}(z,x,h)=(0,\phi(z,x)\xi(h),0)$, which yields, by separation of variables[15]

$$\frac{1}{\gamma}\partial_x^2\phi+\partial_z^2\phi+\frac{\sqrt{\gamma}_z}{\sqrt{\gamma}}\partial_z\phi+q^2\phi=0 \tag{3a}$$

$$-\partial_h{}^2\xi-k_0{}^2n_0{}^2\xi=-q^2\xi \tag{3b}$$

Equation (3a) describes the 2D dynamics in the curved space generated by the thin waveguiding layer, whereas equation (3b) defines the modes of the waveguide. q is a constant with dimensions

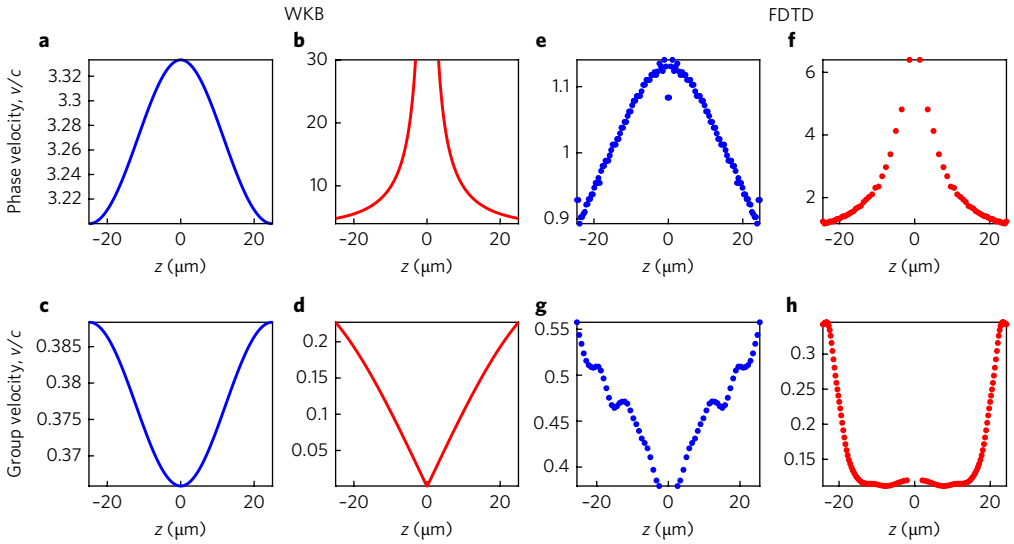

Fig. 2 | Effects of the curvature of space on the phase and group velocities of light in the hollow paraboloid waveguide. a–h, Phase (**a**,**b**,**e**,**f**) and group (**c**,**d**,**g**,**h**) velocities for a low mode (blue) and a high mode (red). In **a**–**d**, analytically calculated velocities by WKB approximation, and in **e**–**h** they are extracted from FDTD simulations. Phase velocity (**a**,**b**,**e**,**f**) is presented as a function of propagation distance. It increases while propagating towards the emulated Schwarzschild radius and decreases when propagating away from it. The higher the mode the stronger the increase in the phase velocity. The group velocity of a pulse of light (**c**,**d**,**g**,**h**) is presented as a function of the propagation distance, and decreases while the mode is propagating towards the emulated Schwarzschild radius. These results show how the curvature affects the phase and group velocities of the light, suggesting a scheme for slow light.

of 1/length that originates from the separation of variables and plays the role of the propagation constant. k_0 and n_0 are the wavenumber and refractive index, respectively. The symmetry enables separation of variables of the form $\phi(x,z)=\frac{1}{\gamma(z)^{1/4}}\psi(z)\int f(k_x)e^{ik_x x}\mathrm{d}k_x$ where we use the k-space representation for the azimuthal part (see comment on the boundary conditions in Supplementary Section 7), yielding an equation for $\psi(z)$ that contains the dependence of the field on z:

$$\psi_{zz}=-\frac{1}{16\gamma^2}(16q^2\gamma^2+3\gamma_z{}^2-4\gamma(4k_x{}^2+\gamma_{zz}))\psi \tag{4}$$

This equation describes a harmonic oscillator, where the effective frequency depends on the metric and its derivatives. Importantly, the eigenmodes of this equation belong to two different regimes of the spatial frequencies and can be either propagating or decaying solutions, depending on $\gamma(z)$. We display these regimes for waves evolving in Flamm's paraboloid in Fig. 1b. As shown, the high bound modes (defined by high spatial frequencies) cannot propagate in the waveguide and are unbound in the vicinity of the emulated Schwarzschild radius.

The effective frequency (in equation (4)) becomes imaginary for these modes in the vicinity of $z=0$ (the effective frequency squared becomes negative), as displayed in Fig. 1b. This means that these modes have an imaginary propagation constant. We solve this equation numerically and find the bound solutions. Notably, ψ has an envelope that depends on the propagation coordinate z, and the rate of phase accumulation also varies with z (see example in Fig. 1c). Near the emulated Schwarzschild radius, the phase accumulation rate of the wavepacket (the envelope ψ) is slower, suggesting that the group velocity is lower.

To obtain a quantitative expression for the phase accumulation as a function of the propagation distance z, we apply the Wentzel–Kramers–Brillouin (WKB) approximation to equation (4) and obtain the shape of the guided modes:

$$\psi(z)\approx\left(\sqrt{\frac{(16q^2\gamma^2+3\gamma_{z'}{}^2-4\gamma(4k_x{}^2+\gamma_{z'z'}))}{16\gamma^2}}\right)^{-\frac{1}{4}}\times \exp\left(\pm i\int\sqrt{\frac{(16q^2\gamma^2+3\gamma_{z'}^2-4\gamma(4k_x^2+\gamma_{z'z'}))}{16\gamma^2}}\,\mathrm{d}z'\right) \tag{5}$$

This expression is general for any metric describing any surface of revolution. It can be regarded as a transfer function for nonparaxial beams propagating within these surfaces. From the expression for the phase, it is straightforward to calculate the phase and group velocities (see Supplementary Sections 5–7 for the calculation and the validity of the approximation). We calculate these velocities for EM waves that are propagating within the surface of the paraboloid described by the metric $\gamma=(z^2/48.56\times10^{-6}+0.935\times10^{-6})^2$ (Fig. 2a–d) and find that—as a mode (of a specific k_x) propagates toward the (emulated) Schwarzschild radius—the phase velocity grows and the group velocity decreases. We verify these results through finite-difference time-domain (FDTD) simulations and study the exact variation of the phase and group velocities of the eigenmodes propagating in the waveguide (Fig. 2e–h). The simulated waveguide is varying adiabatically on the wavelength scale, so the modes evolve adiabatically to the eigenmodes of the following radii, almost without any reflection. To obtain the phase velocity we simulate continuous-wave (c.w.) modes and extract their k_z (longitudinal wavenumber) as a function of z, whereas to calculate the group velocity we simulate the propagation of a light pulse. By monitoring the time evolution of the pulse centre, we extract the group velocity. As expected from the approximate analytic results described above, as the pulse approaches the emulated Schwarzschild radius the phase velocity increases and the group velocity decreases. As shown

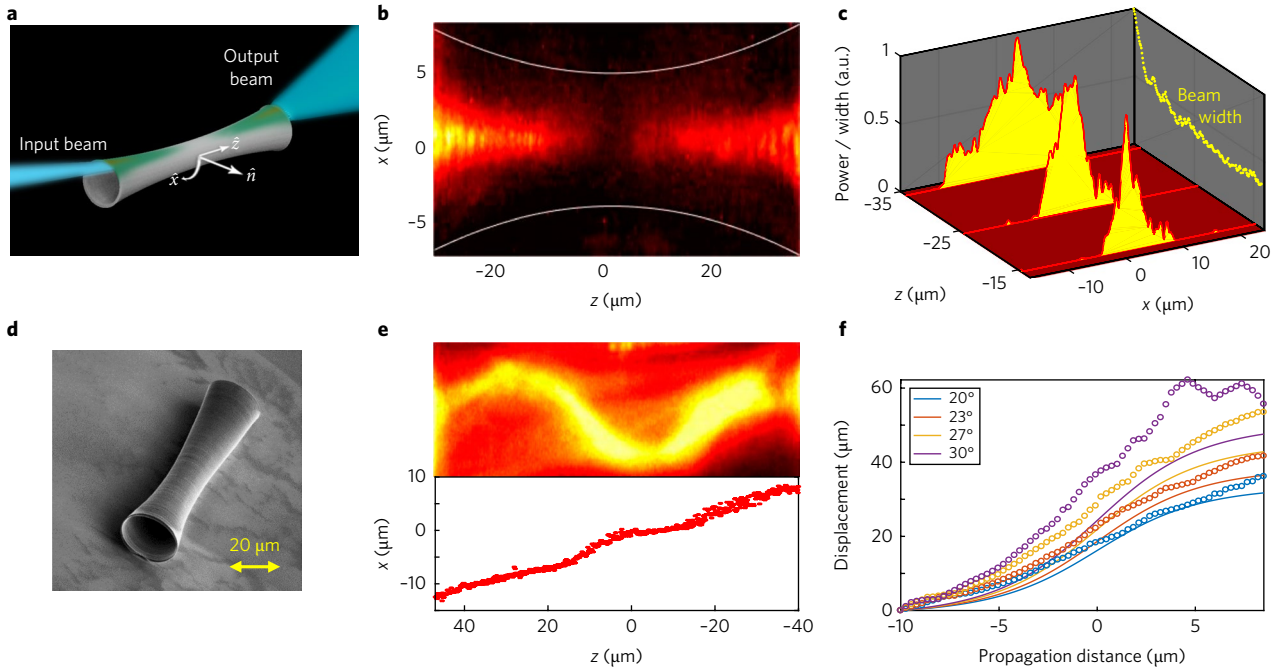

Fig. 3 | Experimental observation of the evolution of an optical beam in the microstructured surface waveguide. a, Schematic of the coupling scheme of the light to the paraboloid waveguide. **b**, Curvature effects on diffraction. The beam narrows as it propagates towards the bottleneck of the structure and power escapes to outside the surface waveguide, when the beam gets near the bottleneck, the power inside the waveguide is considerably depleted. After the bottleneck, the beam reappears and experiences broadening (white lines indicate the borders of the waveguide). **c**, Cross-sections of the beam from **b**. Yellow indicates the evolution of the beam width, which narrows due to the curvature of space. **d**, Scanning electron microscope image of the surface waveguide. **e**, Geodesic trajectory of a beam launched at an initial tilt angle relative to the symmetry axis. Top: experimental observation. Bottom: extracted trajectory. **f**, Comparison of geodesic trajectories calculated from the Schwarzschild metric (equation (8)) (solid lines) and FDTD simulation results (open circles), for beams launched at different angles with respect to the z axis (see legend).

in Fig. 2, there is good qualitative agreement between the analytic prediction and the FDTD simulations in the functional dependence of the group velocity on the propagation distance z. It is important to note that, in the vicinity of the emulated Schwarzschild radius, the dispersion causes some deformation of the pulse, which is the reason for the small peak around $z=0$ (exactly at the emulated Schwarzschild radius) in Fig. 2h. The fact that the group velocity decreases—that is, a pulse of light is slowed down—suggests a new scheme for slow light controlled by the curvature of the surface waveguide only (without any dispersion engineering, as is done in photonic crystals). This result is general and can be used in other curved nanophotonic structures, suggesting a new way to enhance the interaction between light and moving particles.

Experimental realization of curved-space nanophotonics

In what follows, we implement the concepts described above in the laboratory by studying the propagation of EM waves in a 3D hollow waveguide that mimics approximately the structure of Flamm's paraboloid. The surface waveguide has the structure of a paraboloid shaped as two funnels connected back to back. The preliminary results of this work have been presented in conferences[31,32].

Our general fabrication technique for constructing complex structures with 3D features at the nanometric scale is based on the combination of direct laser writing[33] and two-photon fabrication[34], specifically designed for negative-tone photoresists. The method employs two-photon absorption to modify the chemical properties of the photosensitive material in three dimensions, relying on the fact that the two-photon absorption process depends on the intensity of the beam squared, so the laser power can be tuned such that the process creates polymerization of the photoresists only where the laser beam is tightly focused. Namely, in that region, the absorption causes a chemical modification that leads to local polymerization. By scanning the photoresist relative to the fixed focal position, one can write arbitrary 3D structures into the photosensitive material. After a development process, only the predesigned polymerized structure is left. Further details about the fabrication process are provided in Supplementary Section 2. This technique was used to accurately fabricate our predesigned paraboloid surface waveguide with subwavelength resolution, as depicted in Fig. 3d.

This was done using the Nanoscribe commercial 3D laser-writing lithography system equipped with a femtosecond laser at $\lambda=780$ nm wavelength[30]. The fabricated structure is essentially a thin (0.8 μm) hollow tube, 70 μm long, which begins with a radius of 7.4 μm then narrows down (following paraboloidal narrowing) to 4.4 μm, and then broadens again to 7.4 μm radius. The core of the surface waveguide is a 0.8-μm-thick polymerized photoresist (IP-Dip, Nanoscribe) with refractive index of $n\sim1.5$ in the visible wavelength regime, mixed with the fluorescent dye fluorescein. As clearly shown in Fig. 3b,e, the dye is used to visualize the propagation of light within the 3D waveguide layer. The development process consists of soaking for 25 min in propylene glycol monomethyl ether acetate (Sigma-Aldrich) and a further 5 min in isopropyl alcohol to remove all the residual unpolymerized material.

Analysing the modes of this surface waveguide for light at $\lambda=488$ nm wavelength, we find that at its entrance facet, the structure has hundreds of guided modes. As the structure narrows, a large fraction of these guided modes become unbound, transforming into radiation modes. Consequently, light escapes from within the waveguide to its surroundings until, at the bottleneck (which emulates the Schwarzschild radius), only a fraction of the initial power remains within the waveguide. However, as we show in the following, subsequent propagation beyond the bottleneck very efficiently

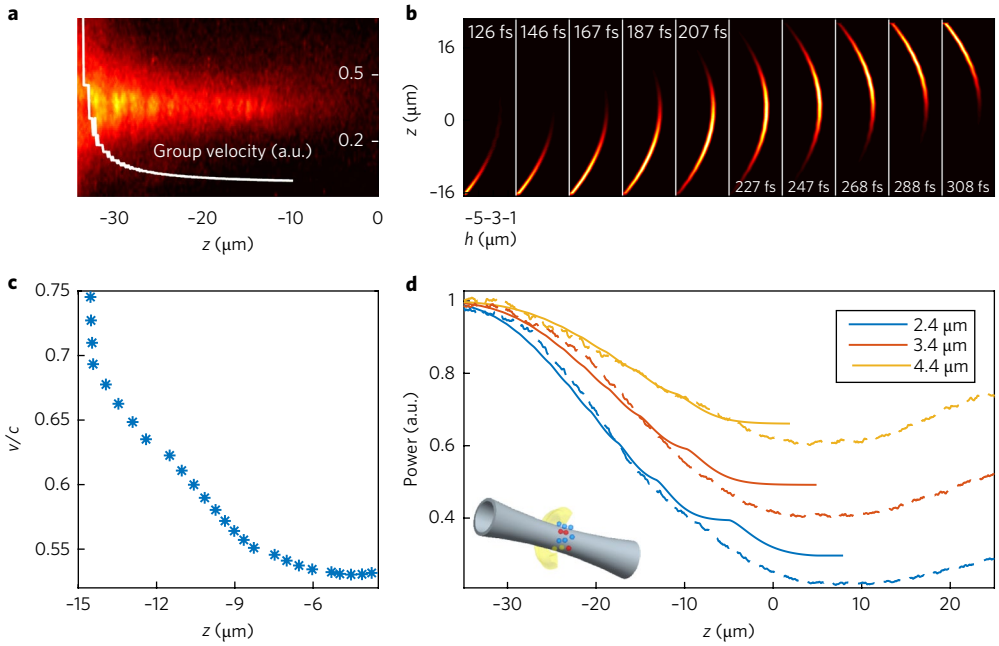

Fig. 4 | Experimental results on light manipulation via space curvature. a, Calculated group velocity extracted from the width evolution of a Gaussian beam in the experiment. In agreement with Fig. 2c,d, the group velocity is decreasing while propagating towards the bottleneck. **b**, Simulated dynamics of a pulse displayed at cross-sections of the paraboloid waveguide for different times. **c**, Group velocity of the pulse extracted from the FDTD simulation displayed in **b**. **d**, Experimentally measured power (dashed lines) of fluorescent light for different propagation distances, as generated solely by the light propagating inside the waveguide, for three different waveguides. The theoretical curves (solid lines) were calculated using equation (5). The maximal radius of all waveguiding structures was 10.4 μm and the minimal radius of each is displayed in the legend. Inset: schematic illustration of a scheme for enhancing the light–matter interaction by exploiting the enhancement of light outside the waveguide and the low group velocity.

recaptures the light into the surface waveguide, to the extent that the power emerging from the exit facet is almost the same as the power coupled into the waveguide at the entrance facet. Physically, this happens because high guided modes of the ring-shaped surface waveguide evolve adiabatically by transforming into radiation modes (which are unbound) while propagating towards the bottleneck, shedding the light out of the guiding layer. After these radiation modes have passed the bottleneck, they transform back into guided modes while sucking the light back into the surface waveguide. This phenomenon is demonstrated in our simulations and experiments, as explained in detail in the following and as displayed in Fig. 4d. The propagation of guided modes within the waveguide can be tracked by observing the fluorescent light emitted by the fluorescein molecules embedded in the waveguide. This is the purpose of mixing the fluorescein molecules into the polymer from which the surface waveguide is fabricated: the $\lambda = 488$ nm light contained in the waveguide is slightly absorbed by these molecules, which subsequently fluoresce at longer wavelengths. The power of the fluorescent light is proportional to the power of the light guided in the surface waveguide.

Control of light via curved-space nanophotonic structures

To demonstrate these concepts in experiments, we excite many high-order modes at the entrance facet of the paraboloid surface waveguide and monitor the fluorescent light emitted from it (Fig. 3b). This process is initiated by tightly focusing a $\lambda = 488$ nm Gaussian beam to a 7 μm spot at the entrance facet and then imaging the fluorescent light with a ×40 objective with NA = 0.45 onto a charge-coupled device. To isolate only the fluorescent light, we placed a 'notch' (band-stop) wavelength filter in front of the camera, centred at $\lambda = 488$ nm. This enabled us to observe only the fluorescent light, which is generated by the optical beam as it propagates inside the waveguide, while avoiding the observation of 488 nm light scattered by random imperfections in the material.

Images of the fluorescent light generated by the light guided within the waveguide are presented in Fig. 3b,c. As can be seen, the beam confined within the waveguiding layer evolves to a narrower beam as it propagates towards the bottleneck, instead of broadening due to diffraction in the curved waveguide. Clearly, this non-paraxial propagation is controlled solely by the curvature. This effect is in accord with the theoretical prediction on the evolution of the eigenmodes propagating towards the emulated Schwarzschild radius: the curvature of space increases the spatial frequencies of the guided modes and as k_x increases, k_z decreases. The beam in the experiment is a superposition of such eigenmodes; the curvature of space maps the input modal constituents to higher spatial frequencies, while the rate of phase accumulation (determined by k_z) slows down. Further details about the experimental set-up and techniques are provided in Supplementary Section 3.

Next, we probe the geodesic trajectories of the light—the shortest trajectories the light is expected to take in a curved space, which naturally depend on the specific curved-space metric. For that purpose, we fabricated a somewhat longer paraboloid waveguide (100 μm long, 10.4 μm maximal radius, 6.4 μm minimal radius). We then focused the input beam at a slanted angle and monitored the geodesics of the light propagating within the surface waveguide. A typical geodesic trajectory of the beam on the paraboloid, as observed in the experiments, is displayed in Fig. 3e. From the experimental image, which gives the projection of the beam trajectory on the imaged plane, we can extract the beam trajectory for the entire propagation distance z within the range of our experiments.

At this point it is instructive to study the correspondence between the evolution of the light in the paraboloid surface waveguide that

we fabricated and the dynamics of the light in the Flamm paraboloid, which we set out to emulate. We do that via FDTD simulations. In the exact simulations, we launch a tightly focused beam at different directions (angle relative to the z axis) and calculate the dependence of the trajectories of the evolving beams on the initial (launch) angle. We compare these to the geodesics arising from the geodesic equation, whose solutions give the shortest paths:

$$\frac{d^2x}{d\lambda^2}+\frac{\gamma_z}{\gamma}\frac{dx}{d\lambda}\frac{dz}{d\lambda}=0 \tag{6}$$

where λ is the affine parameter, which can be the line element. Considering only the forward trajectories, and neglecting back reflections, close to the emulated Schwarzschild radius, we derive the geodesic equation under the paraxial approximation $|dx/dz|<<1$, which yields the approximate line element $d\lambda=dz(1+\frac{1}{2}dx^2/dz^2+O((dx^2/dz^2)^2))$. Substitution of its first order into equation (6) yields the paraxial geodesic equation[17]:

$$\frac{d^2x}{dz^2}+\frac{\gamma_z}{\gamma}\frac{dx}{dz}=0 \tag{7}$$

The solutions to this are

$$x=\gamma(z_i)\frac{x_z}{2}\arctan(z/4r_S)+\gamma(z_i)x_z\frac{z/4r_S}{2(z/4r_S)^2+2}+x_0 \tag{8}$$

Here, z_i is the initial propagation distance at which the beam is launched, and x_z is the initial launch angle relative to the z axis. These calculated geodesics are compared to the trajectories extracted from the FDTD simulations in Fig. 3f.

Our next goal is to extract the velocity from the measurements. Figure 2c displays the evolution of the Gaussian beam launched into the hollow waveguide structure. From this experimental data, we calculate the velocity evolution in the z direction. This procedure is done by fitting a Gaussian profile to the observed beam at each propagation distance. Figure 3c displays the width of the fitted Gaussian beam. Assuming that the shape of the observed beam is approximately Gaussian at each propagation distance, we calculate the effective Rayleigh length as a function of z from the measured beam width. This gives us the phase of the Gaussian beam as a function of propagation distance, enabling a straightforward calculation of the phase and group velocities (for calculation see Supplementary Section 5). (In reality, this assumption means that the beam propagating within the surface waveguide is a Gaussian superposition of hundreds of azimuthal modes that are guided in this waveguide.) As displayed in Fig. 4a, as the Gaussian beam is narrowing while propagating towards the bottleneck, the group velocity decreases, just as expected from the theoretical calculations (Fig. 2). Figure 4a displays the velocity for the left branch ($z<0$) before the beam passes the bottleneck, where the experimental results are cleaner. This experimental result demonstrates the manipulation of the group velocity of the light in this medium exclusively by controlling the curvature. To study this evolution of the group velocity, we also simulated the propagation of a 70 fs pulse with a Gaussian spatial profile, as in the experiment. As is evident from Fig. 4b,c, the group velocity of the pulse decreases as it propagates towards the bottleneck. The reason for the change in the group velocity is the spatial structure, which exhibits evolution due to the curvature, even in homogeneous media. As the pulse propagates towards the bottleneck it also suffers from dispersion effects that change its shape; however, we make sure in our simulations that the position of the pulse can be defined at each propagation distance. From the extracted data, we calculate the group velocity, which is displayed as a function of propagation distance z in Fig. 4c, enabling comparison to the experimental results and to the approximate analytic prediction for a single spatial mode, as displayed in Fig. 2.

Tunnelling through an EM bottleneck

Importantly, as is evident from Fig. 3b, the light guided in the paraboloid surface is almost totally lost around the central region of the paraboloid. There is no fluorescence in the bottleneck, which means that only a small fraction of the power of the light remains guided in that region. However, after the beam passes this bottleneck region, waveguiding is recovered, as manifested by the strong fluorescence in either side of the bottleneck (see also the FDTD simulations of this phenomenon in Supplementary Section 4). This is nicely demonstrated in Fig. 4d, which shows the power carried by the fluorescent light as a function of propagation distance z for several paraboloid-shaped waveguides with different curvatures. The maximal radius of all the waveguides is 10.4 μm, but each waveguide has a different minimal radius (2.4 μm, 3.4 μm, 4.4 μm). The theoretical solid lines in Fig. 4d are obtained by simulations (using the beam propagation method) based on the nonparaxial transfer function we found in equation (5). A dip in the power inside the waveguide is observed in all experimental and theoretical curves for some propagation distance after the bottleneck, caused by this transformation of modes. This happens because, as the diameter of the surface waveguide narrows, high azimuthal modes transform into radiation modes (which are unbound) while propagating towards the bottleneck, shedding light out of the guiding layer. After these radiation modes pass the bottleneck, they transform back into guided modes while sucking the light back into the surface waveguide. (The theoretical simulation method takes into account only forward propagating modes inside the waveguide. For this reason, the theoretical lines predict the power of the beam only until it reaches the bottleneck.) Moreover, as the minimal radius of the paraboloid used in the experiment is smaller, meaning a larger curvature of space, a higher fraction of the power is radiating outside the waveguide. It is important to emphasize that this effect depends on the first and second derivatives of the waveguide radius and it is in its nature very nonparaxial (in the paraxial limit, only the radius affects light evolution[17]).

Controlling the light coupling from the guided modes into the radiative modes, which extends outside the waveguiding layer (as appears in Fig. 4d), together with the low group velocity in the vicinity of the bottleneck, can be useful for many experiments involving light and matter in tightly confined environment, such as nanowires or microcavities coupled to atoms positioned just outside their exterior, as in the experiments by Kimble's group[35,36] and in the recent experiments by Dayan's group[37]. It is important to note that we have an analytical expression for the transfer function of wavepackets propagating within curved surfaces (equation (5)) that depends on the metric determinant and its derivatives. As such, an optimization process can be applied to any specific application. Moreover, any material that has specific properties that are important for a specific quantum interaction scheme can be structured to a specific geometry without altering its properties (changing its resonances and so on). It is important to note that the materials used in this Article are only one example of many possibilities, and our structures can be transformed into structures of different materials using post-processing methods. Moreover, a structure with asymmetric curvature in the z direction can be designed to provide another mechanism to control how much of the incoming energy can be coupled to the output, by controlling the percentage of the radiated energy that will be captured after the bottleneck. This property can be useful in waveguide devices.

To conclude, we have demonstrated a new platform for engineering curved-space settings where the curvature of the structure controls the evolution of light, determining the phase and group

velocities, transforming guided modes into radiative (unbound) states and back, and more. On the fundamental side, this platform makes it possible to emulate various effects related to curved space, and to study them experimentally in the regime where the curvature is comparable to the wavelength of the light. On the applications side, this method paves the way for the design, fabrication and optimization of a new class of 3D nanophotonic devices. Our methodology facilitates the precise design and fabrication of subwavelength-scale 3D arbitrary constructions, including subwavelength features at nanometric precision. The ability to dictate the exact curved geometry in which the light will propagate makes it a powerful tool for studying unique effects that were never before accessible for experimental research. The realization of Flamm's paraboloid is only one example out of many more possible directions. We believe that the robustness of the fabrication process will enable the generalization of this type of photonic structure to various applications and systems.

Data availability. The data that support the plots within this paper and other findings of this study are available from the corresponding author upon reasonable request.

Received: 13 January 2017; Accepted: 8 August 2017;
Published online: 29 September 2017

References

1. Laundau, L. D. & Lifshitz, E. M. *The Classical Theory Of Fields* (Butterworth-Heinemann, Oxford, 1975).
2. Leonhardt, U. & Philbin, T. G. General relativity in electrical engineering. *New J. Phys.* **8**, 247 (2006).
3. Cai, W. & Shalaev, V. *Optical Metamaterials Fundamentals and Applications* (Springer, New York, 2010).
4. Grbic, A. & Eleftheriades, G. V. Overcoming the diffraction limit with a planar left-handed transmission-line lens. *Phys. Rev. Lett.* **92**, 117403 (2004).
5. Schurig, D. et al. Metamaterial electromagnetic cloak at microwave frequencies. *Science* **314**, 977–980 (2006).
6. Alù, A. & Engheta, N. Multifrequency optical invisibility cloak with layered plasmonic shells. *Phys. Rev. Lett.* **100**, 113901 (2008).
7. Ergin, T., Stenger, N., Brenner, P., Pendry, J. B. & Wegener, M. Three-dimensional invisibility cloak at optical wavelengths. *Science* **328**, 337–339 (2010).
8. Chen, X. et al. Macroscopic invisibility cloaking of visible light. *Nat. Commun.* **2**, 176 (2011).
9. Shalaev, V. M. Optical negative-index metamaterials. *Nat. Photon.* **1**, 41–48 (2007).
10. Alù, A., Silveirinha, M. G., Salandrino, A. & Engheta, N. Epsilon-near-zero metamaterials and electromagnetic sources: tailoring the radiation phase pattern. *Phys. Rev. B* **75**, 155410 (2007).
11. Silveirinha, M. & Engheta, N. Design of matched zero-index metamaterials using nonmagnetic inclusions in epsilon-near-zero media. *Phys. Rev. B* **75**, 075119 (2007).
12. Edwards, B., Alù, A., Young, M. E., Silveirinha, M. & Engheta, N. Experimental verification of epsilon-near-zero metamaterial coupling and energy squeezing using a microwave waveguide. *Phys. Rev. Lett.* **100**, 033903 (2008).
13. Naik, G. V., Shalaev, V. M. & Boltasseva, A. Alternative plasmonic materials: beyond gold and silver. *Adv. Mater.* **25**, 3264–3294 (2013).
14. Smolyaninov, I. I., Smolyaninova, V. N., Kildishev, A. V. & Shalaev, V. M. Anisotropic metamaterials emulated by tapered waveguides: application to optical cloaking. *Phys. Rev. Lett.* **102**, 213901 (2009).
15. Batz, S. & Peschel, U. Linear and nonlinear optics in curved space. *Phys. Rev. A* **78**, 043821 (2008).
16. Schultheiss, V. H. et al. Optics in curved space. *Phys. Rev. Lett.* **105**, 143901 (2010).
17. Bekenstein, R., Nemirovsky, J., Kaminer, I. & Segev, M. Shape-preserving accelerating electromagnetic wave packets in curved space. *Phys. Rev. X* **4**, 011038 (2014).
18. Genov, D. A., Zhang, S. & Zhang, X. Mimicking celestial mechanics in metamaterials. *Nat. Phys.* **5**, 687–692 (2009).
19. Narimanov, E. E. & Kildishev, A. V. Optical black hole: broadband omnidirectional light absorber. *Appl. Phys. Lett.* **95**, 041106 (2009).
20. Chen, H., Miao, R.-X. & Li, M. Transformation optics that mimics the system outside a Schwarzschild black hole. *Opt. Express* **18**, 15183–15188 (2010).
21. Fernández-Núñez, I. & Bulashenko, O. Anisotropic metamaterial as an analogue of a black hole. *Phys. Lett. A* **380**, 1–8 (2016).
22. Philbin, T. G. et al. Fiber-optical analog of the event horizon. *Science* **319**, 1367–1370 (2008).
23. Belgiorno, F. et al. Hawking radiation from ultrashort laser pulse filaments. *Phys. Rev. Lett.* **105**, 203901 (2010).
24. Barceló, C., Liberati, S. & Visser, M. Analogue gravity. *Living Reviews in Relativity* **14**, 3 (2011).
25. Demircan, A., Amiranashvili, Sh. & Steinmeyer, G. Controlling light by light with an optical event horizon. *Phys. Rev. Lett.* **106**, 163901 (2011).
26. Sheng, C., Liu, H., Wang, Y., Zhu, S. N. & Genov, D. A. Trapping light by mimicking gravitational lensing. *Nat. Photon.* **7**, 902–906 (2013).
27. Karen, E. et al. Nonlinear optics of fibre event horizons. *Nat. Commun.* **5**, 4969 (2014).
28. Wang, S. F. et al. Optical event horizons from the collision of a soliton and its own dispersive wave. *Phys. Rev. A* **92**, 023837 (2015).
29. Bekenstein, R., Schley, R., Mutzafi, M., Rotschild, C. & Segev, M. Optical simulations of gravitational effects in the Newton–Schrödinger system. *Nat. Phys.* **11**, 872–878 (2015).
30. http://www.nanoscribe.de/
31. Bekenstein, R. et al. Curved space nanophotonics inspired by general relativity. In *Conference on Lasers and Electro-Optics* paper FW1D.2 (Optical Society of America, 2016).
32. Kabessa, Y. et al. Nanophotonic structures constructed in a curved space inspired by general relativity concepts. In *Advanced Photonics* paper ITu1A.7 (Optical Society of America, 2016).
33. Kawata, S., Sun, H.-B., Tanaka, T. & Takada, K. Finer features for functional microdevices. *Nature* **412**, 697–698 (2001).
34. Maruo, S., Nakamura, O. & Kawata, S. Three-dimensional microfabrication with two-photon-absorbed photopolymerization. *Opt. Lett.* **22**, 132–134 (1997).
35. Aoki, T. et al. Observation of strong coupling between one atom and a monolithic microresonator. *Nature* **443**, 671–674 (2006).
36. Dayan, B. et al. A photon turnstile dynamically regulated by one atom. *Science* **319**, 1062–1065 (2008).
37. Shomroni, I. et al. All-optical routing of single photons by a one-atom switch controlled by a single photon. *Science* **345**, 903–906 (2014).

Acknowledgements

This research was supported by the Israeli Ministry of Science and Technology and by the US Air Force Office of Scientific Research. R.B. acknowledges support from the Adams Fellowship Program of the Israel Academy of Sciences and Humanities and the support of the National Science Foundation through a grant to ITAMP. Y.K. and A.J.A. thank Y. Garcia at the Brojde Center for Innovative Engineering and Computer Science for advice and assistance in using the Nanoscribe system.

Author contributions

All authors contributed significantly to this work.

Competing interests

The authors declare no competing financial interests.

Additional information

Supplementary information is available for this paper at doi:10.1038/s41566-017-0008-0.

Reprints and permissions information is available at www.nature.com/reprints.

Correspondence and requests for materials should be addressed to R.B. or Y.K.

Publisher's note: Springer Nature remains neutral with regard to jurisdictional claims in published maps and institutional affiliations.